

# Scatterfield microscopy for extending the limits of image-based optical metrology

Richard M. Silver,\* Bryan M. Barnes, Ravikiran Attota, Jay Jun, Michael Stocker, Egon Marx, and Heather J. Patrick

National Institute of Standards and Technology, Gaithersburg, Maryland 20899, USA

\*Corresponding author: silver@nist.gov

Received 25 October 2006; revised 16 March 2007; accepted 19 March 2007;  
posted 22 March 2007 (Doc. ID 76383); published 20 June 2007

We have developed a set of techniques, referred to as scatterfield microscopy, in which the illumination is engineered in combination with appropriately designed metrology targets to extend the limits of image-based optical metrology. Previously we reported results from samples with sub-50-nm-sized features having pitches larger than the conventional Rayleigh resolution criterion, which resulted in images having edge contrast and elements of conventional imaging. In this paper we extend these methods to targets composed of features much denser than the conventional Rayleigh resolution criterion. For these applications, a new approach is presented that uses a combination of zero-order optical response and edge-based imaging. The approach is, however, more general and a more comprehensive set of analyses using theoretical methods is presented. This analysis gives a direct measure of the ultimate size and density of features that can be measured with these optical techniques. We present both experimental results and optical simulations using different electromagnetic scattering packages to evaluate the ultimate sensitivity and extensibility of these techniques.

*OCIS codes:* 110.0180, 050.1940, 120.3940.

## 1. Introduction

Recently, there has been significant research investigating potential technologies to meet the challenges of imaging very small device-sized targets used in feature-to-feature overlay metrology and linewidth measurements for the semiconductor and nanoelectronics manufacturing industries [1,2]. Tighter manufacturing tolerances are driving the need to use device-sized targets, which more closely emulate the characteristics of the actual features of interest printed on the wafers. There also remains a lingering question as to how much longer optical methods will provide accurate metrology outputs on very small feature sizes [3]. Often, the high throughput and lower cost of optical systems make them the measurement techniques of choice, provided they are capable of robust measurement of the features of interest.

Most obstacles encountered in leading-edge bright-field optical metrology can be divided into two sepa-

rate, related areas: (1) the challenge of whether or not a feature can be resolved and (2) whether one can make a robust optical image-based measurement. The first challenge is whether a feature or signal can be resolved or imaged and whether there is appropriate sensitivity to changes in the measurand. This lends itself to using physics-based electromagnetic scattering models and the necessity to evaluate the optical response and sensitivity to changes in an imaging target. The second challenge relates to the continued application of edge- and image-based optical techniques as opposed to more complex optical signatures that require model-based interpretation.

In previous publications we described our implementation of the scatterfield microscopy technique, which generally involves engineering the illumination in a Köhler illuminated bright-field microscope in combination with structured samples [4,5]. To investigate the limitations of this approach we have modeled targets with linewidth dimensions down to 10 nm. Fundamentally there are no significant roadblocks to measuring isolated features 1/20th the size

of the measurement wavelength and, using well-engineered illumination and target designs, very good signal-to-noise ratios can be achieved. A number of examples presented in [6] utilize both theoretical techniques and experimental implementations to develop and demonstrate excellent optical response to small subwavelength features. The problem, however, becomes more challenging when the features become densely positioned. The optical response from isolated small features is quite different from that of small features in dense arrays.

#### A. Zero-Order Imaging

In this paper we present a new approach to optical measurements of very dense arrays. As an example, we analyze 50 nm size features, which are spaced 250 nm apart with 546 nm wavelength light. The typical optical response to an array filling the field of view at the 546 nm measurement wavelength is a flat or constant intensity pattern with no optical intensity variation. The cause of this constant intensity pattern is that only specular or zero-order light is reflected. That is, the collection optics are only capturing the specular reflected component; either higher-order terms do not exist or they are outside the collection aperture. We have developed an approach to image the sample in this situation. If features are placed close enough together they locally reflect only the zero-order component, resulting in a flat intensity response across the image plane. However, if the target actually has a finite overall dimension within the field of view, then the edges of the target will diffract higher-order light. Several targets can be co-placed in the field of view having this characteristic. This results in a conventional image where each small array is delineated only by its boundary edges, although the internal signal from within the edges is attributed to only zero-order reflected light. We refer to this as zero-order imaging.

The result is that small groupings of features with subwavelength dimensions can give an excellent localized optical response as a function of position across the image plane. Their optical response is a combination of the higher-order edge response and a zero-order central intensity. These targets have applications in feature-to-feature overlay and critical dimension linewidth metrology. For overlay applications the arrayed targets can act as individual objects, which are well suited for edge detection algorithms and correlation functions commonly used to determine relative feature positions for image-based techniques.

#### B. Back Focal Plane Scanning

In addition to the imaging of dense features as described above, a more complex approach is to scan an aperture in a conjugate back focal plane, resulting in illumination of the sample at specific chosen angles. More rigorously, in the Köhler illumination configuration used in our hardware, a small cone of plane waves illuminates the sample from a selected direction (the primary angle of illumination), which is

ultimately limited in our current design by the collection numerical aperture. As the aperture is scanned in a conjugate illumination back focal plane, the primary angle of illumination changes and images are captured at each illumination angle. The images captured are the result of two different phenomena. Either a dense array is imaged and only a constant intensity is captured at the image plane, or for less dense targets the image will contain higher-order optical response information and appear as a conventional optical image of an array. In either case, the intensity image is captured and a total or average intensity as a function of illumination angle or aperture position is determined. This approach is similar to that used in scatterometry and is essentially a combination of scatterometry and bright-field optical microscopy (giving rise to the name scatterfield microscopy). Figure 1 shows the basic hardware configuration. The hardware and instrumentation used in the research reported in this paper are described in detail elsewhere [7]. Figure 1 is a schematic representation of the illumination configuration and combined collection and illumination optical train. The actual optical column involves a number of relay lens groups and magnification lens groups designed to provide an adequate conjugate back focal plane size with an acceptable level of aberration.

We first present applications of the technique to large continuous arrays of features and evaluate their sensitivity to changes in feature geometry and linewidth. Then we present results from the measurement of a group of arrays for use in combined optical metrology applications. Although comparison of theoretical analysis and experimental data will be presented, this is not intended to be a comprehensive treatment of experimental and theoretical comparisons. The results presented here do, however, give a concrete indication as to what the ultimate sensitivity and resolution limits are for optical-based metrology.

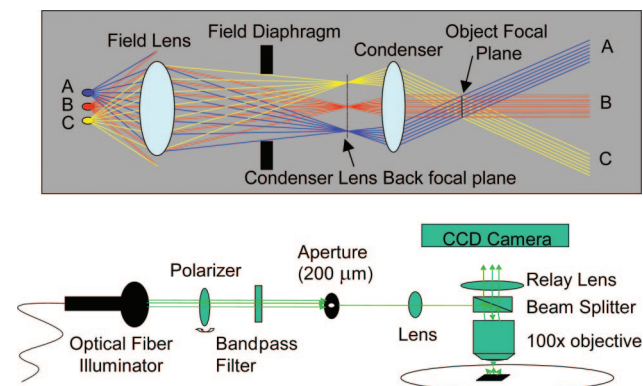


Fig. 1. (Color online) Simplified schematic of the optical configuration. The upper figure is a conceptual drawing of the illumination path demonstrating how access to a conjugate back focal plane enables selective angular illumination or more general illumination engineering. The lower part of the figure shows the layout of the laboratory implementation.

### C. Test Sample Characterization

To develop the methods described in this paper, etched silicon target arrays were fabricated at SEMATECH with different process stacks. These targets include a variety of large arrays having overall dimensions from  $20\ \mu\text{m} \times 20\ \mu\text{m}$  up to  $100\ \mu\text{m} \times 100\ \mu\text{m}$ . The large array data presented in this paper are from the  $100\ \mu\text{m} \times 100\ \mu\text{m}$  arrays. These targets are etched 230 nm deep in silicon and have sidewall angles measured using atomic force microscopy (AFM). These targets are referred to as the etched silicon targets and were designed as part of the Overlay Metrology Advisory Group (OMAG 3 reticle set) [8]. A second set of arrayed targets were prepared having a similar set of array designs and dimensions but were prepared by etching a 100 nm thick amorphous silicon layer on a 2 nm gate oxide. These wafers (OMAG 4 reticle set) resulted in better control of the sidewall geometry and allowed for overetching the lines, yielding smaller critical dimensions (CDs). The OMAG 4 reticle set also has a set of arrayed overlay targets, the National Institute of Standards and Technology (NIST) high-resolution overlay targets, presented in Section 5 of this paper.

The wafers were exposed using a focus exposure matrix (FEM). This results in linewidths that varied by less than 1 nm from die to die and provides excellent targets for testing sensitivity to small changes in feature size. The FEM did result in some variation of the sidewall angles. The data presented in the following sections are from selected die that yield a total change in linewidth across the dies chosen of 6 nm for the 300 nm pitch arrays and 12 nm for the 600 nm pitch arrays.

AFM and scanning electron microscopy (SEM) were used to measure the linewidths and pitch values for use in determining the starting-point simulation parameters. There are minor disagreements between the SEM measurements and the AFM measurements, which remain unresolved. Depending on the linewidth and sidewall angle in particular, the disagreement ranged from insignificant to as much as 25 nm. However, both methods showed approximately the same variation in linewidth across a given range of die but offset with respect to one another. The discrepancies may at least in part be due to the variation in sidewall angle and the different measurement algorithms used.

## 2. Background Compensation and Signal Normalization

Data were acquired using the configuration shown schematically in Fig. 1. An aperture is scanned in a conjugate back focal plane of the objective in the illumination optical path. An image is acquired for selected positions of the aperture across the back focal plane. Thirty-one positions were routinely used, which spanned illumination angles greater than the objective numerical aperture (NA) could accept. An image is obtained for each aperture position with the corresponding illumination configuration having a

small cone of plane waves nominally 0.11 NA in size. That is, a small aperture of  $200\ \mu\text{m}$ , equivalent to an on-axis NA of 0.11, is scanned across the back focal plane, which is approximately 2 mm in size. The range of angles for the cone of illuminating plane waves is  $\pm 6^\circ$ , and this is scanned from more than  $+60^\circ$  to  $-60^\circ$  (the primary angle) with respect to the optical axis. The collection NA is 0.95.

There are several contributions to the target image and background signal that require normalization. First, there is a dark current that is removed from each image. There are target-independent variations in the illumination intensity across the field of view. There are also variations in the overall intensity at each aperture position, due to the angular dependence of the illumination and transmission in the microscope optics. To correct for these effects, at each occurrence of an acquisition (for each illumination angle), a blank background image is acquired at a nearby site on the silicon. The intensity of a target image is then normalized to that of its background image using a pixel-by-pixel array method.

The use of a bare silicon background image as reference enables us to calculate a correction for the polarization and angular dependence of the illumination and the transmission through the microscope optics. This correction is then applied to the target image to convert the intensity of a target image at a given illumination angle to reflectance of the target at that angle. This approach works well for zero-order imaging, where, for both the target and for bare silicon, each illumination angle maps to a single specular reflection angle. However, the correction calculated from bare silicon has limited application to targets with higher diffraction orders because in this case the target diffracts light at multiple angles for a single illumination angle, and the transmission correction for the higher orders is not obtained from the bare silicon correction.

Figure 2 shows the normalization sequence for evaluating the polarization-dependent transmission through the imaging system. The upper panels show unpolarized and polarized intensity as a function of angle, for a blank area of silicon, measured at the image plane with a CCD camera. In the lower panels the theoretical curves for silicon reflectivity as a function of angle are shown. The theoretical curves are calculated from Fresnel reflectance theory, using the optical constants of silicon [9]. The difference between the upper and lower panels is the direct effect of polarization-dependent transmission through the optics as a function of angle. The TE polarization is nearly flat on average, whereas the TM polarization is closer to the expected nominal behavior. The experimental data for a target can only be compared to theory after this effect has been properly compensated. For each polarization, a correction curve is derived by dividing the lower (calculated) curve for silicon shown in Fig. 2 by the upper (measured) curve. The reflectance of a target versus illumination angle is then given by its measured intensity versus angle, multiplied by the correction curve. Figure 3 shows typical target data as acquired and following the cor-

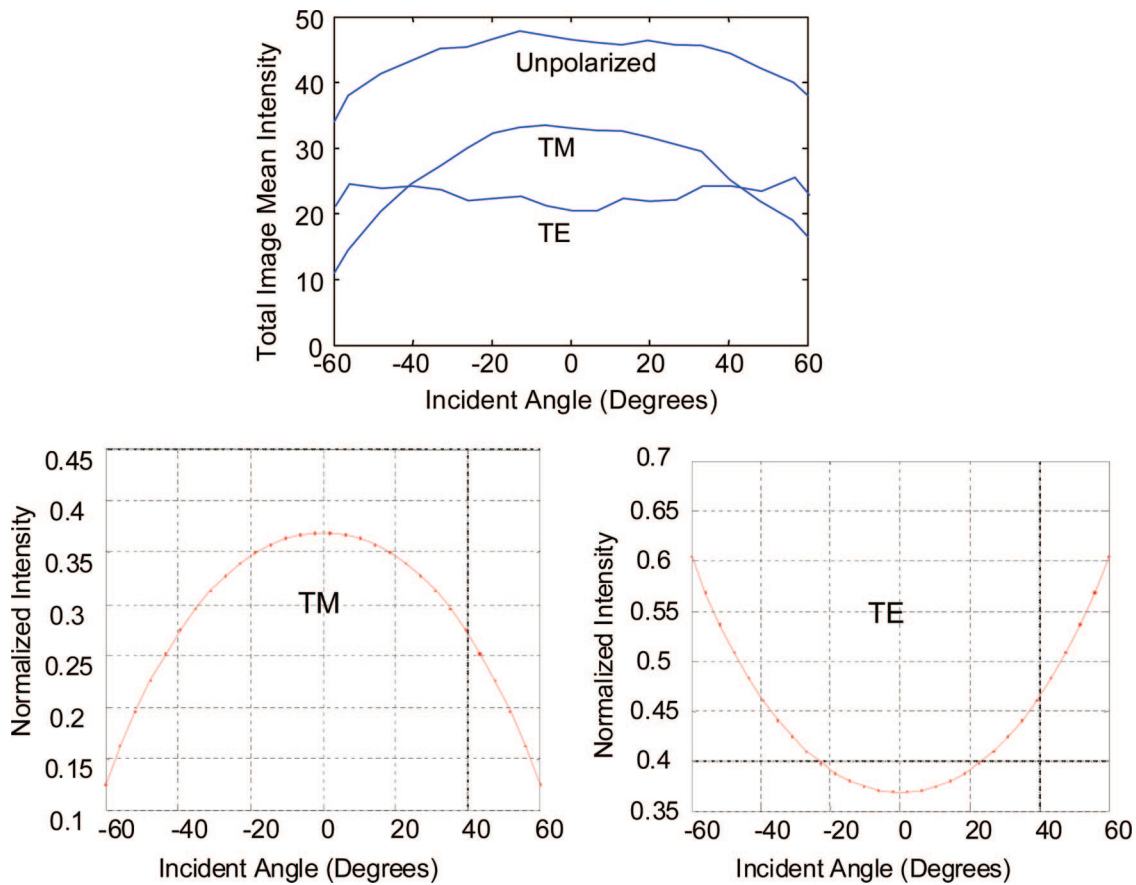


Fig. 2. (Color online) Background intensity data is acquired for each image as a function of angle, plotted in the upper panel for the unpolarized case and both polarizations. A point-by-point matrix correction is used to normalize the angle-resolved background data to account for the angle-dependent intensity variation. The reflected light is then normalized using the theoretical angle-dependent silicon reflectivity curves shown in the lower part of the figure. This approach is essential to normalize the angle-resolved data correctly so it can be compared to simulations.

rection. The data in Fig. 3 are normalized on a point-by-point basis by correcting for the intensity error observed at each angle relative to that based on that observed. The finite angular illumination approach allows us to accurately measure and quantify the angular dependence of the illumination and transmission through the optical train. This is an important effect to quantify any time optical images are compared to theory since this polarization dependence results in a substantial error, particularly for the TE-polarized light. In subsequent measurements this has been confirmed through measurements of the polarized light directly on the exit of the objective lens.

### 3. Full-Field Angle Scans

In the first part of this section the data described were acquired from OMAG 3 arrays, which fill the field of view. The data were acquired by collecting conventional images at the image plane with a CCD camera. A window or kernel is placed in the image and an average intensity per unit area determined. This mean intensity is evaluated for each angle of illumination. Two types of results are observed. The first result occurs when the pitch values are large

enough for higher-order optical information to be scattered and collected by the optics. The second, alternative result is a flat intensity across the field containing only zero-order optical information. The aperture is scanned in the back focal plane across a large enough distance to clip the aperture at the extremes, and as a result the intensity falls off for positions in the back focal plane that correspond to angles of illumination greater than  $60^\circ$ .

Figure 3 shows four sets of curves, the top two are for TE polarization and the bottom two for TM polarization data. This figure shows the 300 nm pitch array with linewidths varying from 150 to 156.5 nm based on the SEM values. The data shown on the left side of the figure are not yet normalized for the silicon reflectivity although they have been processed for background and dark current compensation. The curves show clear sensitivity to nanometer changes in linewidth. These data are repeatable and show a monotonic response to linewidth changes.

The data on the right side of Fig. 3 show the same results after they have been corrected for the silicon reflectivity. The correction effectively scales the data, which in this case increases the dynamic range in the

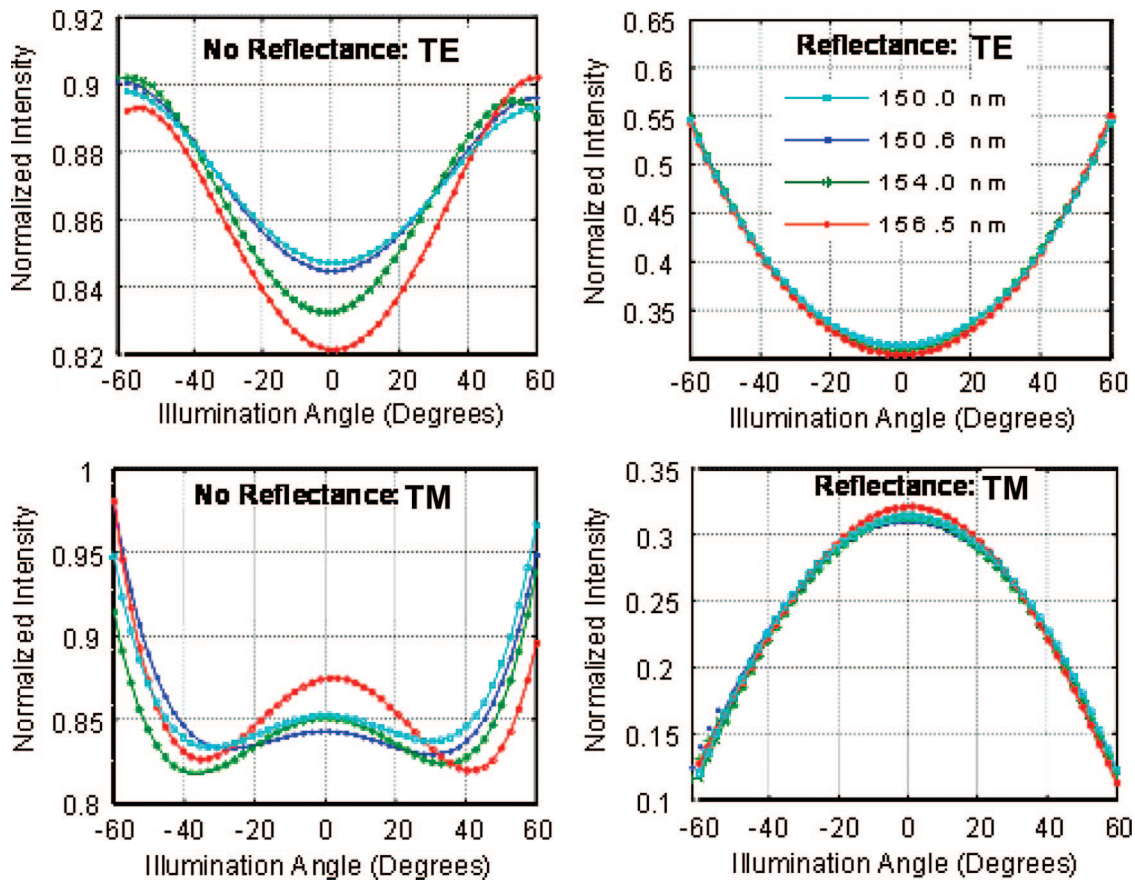


Fig. 3. Experimental data before and after normalization. TE polarization is on top and TM is shown on the bottom. The vertical axes are units of normalized intensity and the horizontal axes are illumination angle in degrees. The data show good sensitivity to nanometer changes in linewidth. The data on the left are presented prior to normalization and show good sensitivity to small changes in line width. The data on the right side have been normalized to the background. The normalization process changes the dynamic range and results in the apparent loss of sensitivity, which can be easily regained by focusing on a smaller range of angles. The normalization process is essential when comparing theory to experiment.

graph and makes the curves appear closer to each other in value relative to the raw, uncorrected data.

A similar set of data is shown in Fig. 4 for lines with a nominal pitch of 600 nm. In this case the initial image shows an optical response that includes intensity variation throughout the field of view. The same approach of applying a window and running an algorithm to calculate an average integrated intensity per unit area can be used, followed by graphing the average integrated intensity as a function of angle. Results are shown for both experimental data and a series of simulations. The simulations cover a broad range of linewidths based on the range of SEM and AFM measurements. In both cases there are offsets between the SEM and AFM data, which is the reason such a large range of linewidth parameters were used in the initial simulations.

Comparison of the TE data in Fig. 4 shows qualitative agreement in intensity patterns between the experimental range of linewidths and those in the simulation near 155 nm. Similarly, comparing the TM data and simulations show a qualitative trend of agreement with the simulation data in the 145–155 nm range. These simulations are intended to

identify the feature dimensions to within 10 nm, where a more comprehensive analysis can be run, which includes a parametric evaluation of the parameter space to determine the effects of other physical parameters such as small variations in line height, sidewall angle, or optical constants. These parametric effects are discussed in more detail in [10], where a fractional factorial approach was used to optimize the simulation parameters.

The theoretical methods used have been described in detail elsewhere [11,12]. The first method used here was the rigorous coupled waveguide analysis (RCWA). Briefly, the RCWA model uses a modal method called the analytic waveguide method with an infinite grating. It calculates the eigenmodes in a waveguide decomposition of the scattering essentially exactly. The fields are expanded in terms of the eigenmodes and then calculated analytically without use of a Fourier series. A matrix relates the generalized Fourier series of the fields in one  $z$  layer to those in an adjacent  $z$  layer using boundary conditions [10]. The finite-difference time domain computation involves a time-based leapfrog method where updating equations alternate between electric field and mag-

## 230 nm tall Si lines, 600 nm pitch (silicon reflectivity and background normalized)

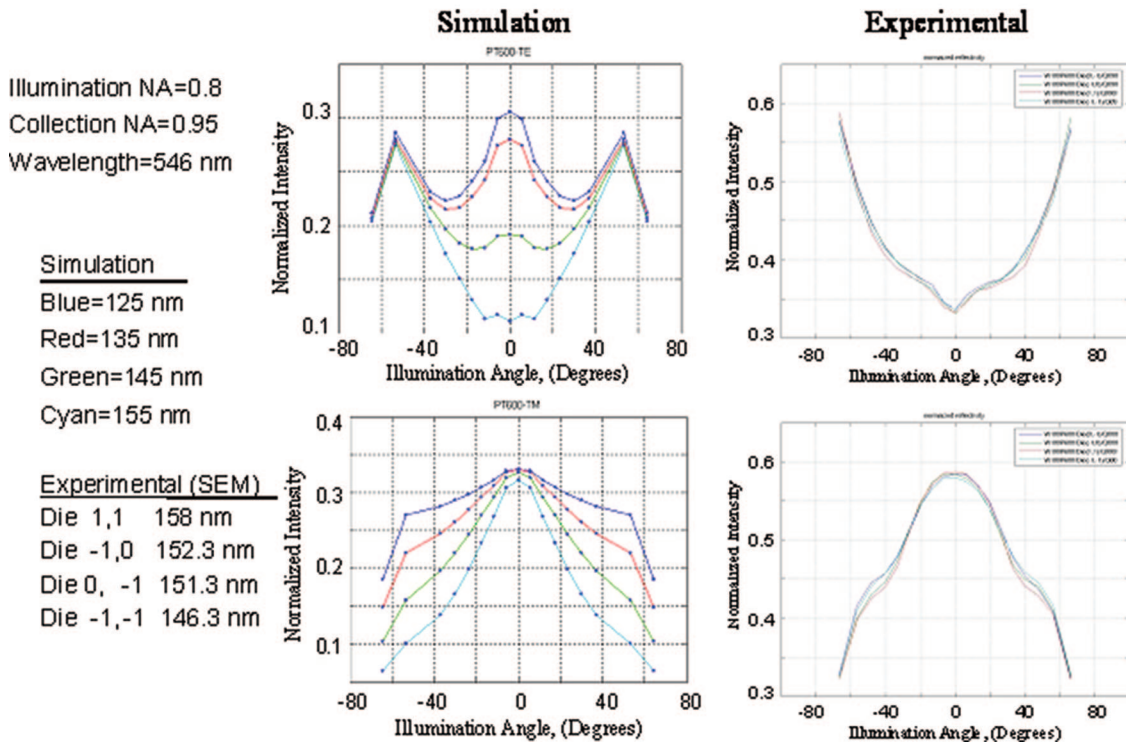


Fig. 4. (Color online) Data on the left are simulation results and the right side shows experimental results. The vertical axes are units of normalized intensity. The simulations span the range of CD values measured with the AFM and SEM. The experimental data are silicon corrected and compare most favorably with the simulations between 145 and 155 nm. Subsequent work with higher-resolution simulation steps confirms these results.

netic field calculations. To do so, Maxwell's equations are transformed from their vector, differential form into difference equations. For each time step,  $x$ ,  $y$ , and  $z$  components of the  $E$  field are evaluated at the time step. Similarly, the three  $H$ -field components are evaluated between time steps, requiring a total of six calculations [12].

There are a number of parameters that affect the optical image and the optical response of a target to a particular illumination configuration. The optical constants  $n$  and  $k$  have a well-known effect on the electromagnetic scattering from a target. The illumination NA as well as the collection NA also have substantial effects on the intensity response and resolution. We have worked extensively to advance and quantify the detailed theoretical understanding of these numerous parametric effects on the optical scattering and imaging processes. One important advantage of using the scanned aperture approach described here is that errors introduced to the illumination and imaging process can be evaluated in a simplified form and as a function of illumination angle. This has allowed us to quantify and normalize the substantial polarization effects in the optical train.

In addition, we have previously shown that the illumination NA can play a significant role in enhancing the optical response. The measurement wavelength affects the conventional resolution seen in an

image but also plays a crucial role in the more complex optical phenomena seen in [6]. In this work, light is scattered off an array of lines and strong electromagnetic field oscillations in the intensity are observed above the sample. The details of these oscillations in the electromagnetic intensities can be measured and attributed directly to the line geometry. The target pitch dimension in this work was also shown to couple strongly with measurement wavelength and to have a similar effect on the optical response. The work presented here builds directly on those concepts.

Analysis of these data shows nanometer sensitivity to the small differences in the die-to-die variation in linewidth. The simulations show that, given the parametric inputs used, the lines are closest to the 145–155 nm linewidths, in qualitative agreement with the values measured by SEM. The simulations also show significant theoretical sensitivity to geometrical changes for these targets and that this technique is a candidate for measuring changes in geometrical shape.

#### 4. High-Resolution Arrayed Targets

Although the above discussion and results were focused on sensitivity to changes in linewidth, geometry, and the ability to obtain an optical signal from small features, these results have significant implications for optical overlay metrology. In developing

applications of this high-resolution optical method it is strongly desirable to enable both direct image-based measurements when desired (e.g., for feature-to-feature overlay) while permitting more complex model-based signal analysis for critical dimension and linewidth applications. In this section we will apply the same scanning aperture techniques described above to an array of targets within the field of view.

An additional set of targets were analyzed from the OMAG 4 wafer set and used to obtain the results shown in the next section. The etched amorphous silicon process allowed us to achieve smaller linewidths. We did not prepare a characterized set of focus exposure die since this part of the study was intended to test and evaluate the technique at smaller feature dimensions. The features were, however, well characterized again by AFM and SEM to determine a linewidth window and sidewall geometry.

#### A. Overlay Targets

A set of targets was designed that consisted of an array of small line arrays as shown in Fig. 5. Unlike the previous targets, these targets are intended to allow measurement of the relative position or overlay between two layers that can also be imaged using the zero-order imaging approach. In the figure, the outer line sets are from one photolithographic level and the inner line sets are from a second photo level. The current target designs are sets of eight lines with a variety of line lengths, line set separations, and line widths to allow investigation of these parameters on

target performance. This figure shows one variation of the target design. For this target design, the optical response to individual line sets includes high-order optical content reflecting from the central part of the lines, as shown in Fig. 5(b). Alternatively, a second set of targets is imaged in the zero-order mode as shown in Fig. 6. In this figure, only zero-order specular reflection occurs from the central target region of an individual line set, although the individual line sets do reflect higher-order optical content from their edges.

Figures 5 and 6 show typical applications of the algorithms, which select and generate the window or kernel for use in analysis. The algorithm applied uses a horizontal window as shown in the figures, which is typically 2–5  $\mu\text{m}$  in height (100–250 pixels vertically), which is then collapsed into a single profile. This algorithm is applied to every image acquired at each angle. A resulting profile from one image is shown in Fig. 5(c). Note the number of oscillations in the central region for each line set. In Fig. 6 the three bright oscillations are an interference effect involving the eight lines and the edges that comprise the target, not higher-order optical content from the interior region of the eight lines.

An interesting enhancement to the measurements can be made by illuminating at high angles. This can contribute, depending on the target and measurement wavelength, higher-order diffraction content to the image. A theoretical example is shown in Fig. 7, where the sample is illuminated at four different angles, from normal incidence to approximately  $60^\circ$ , resulting at

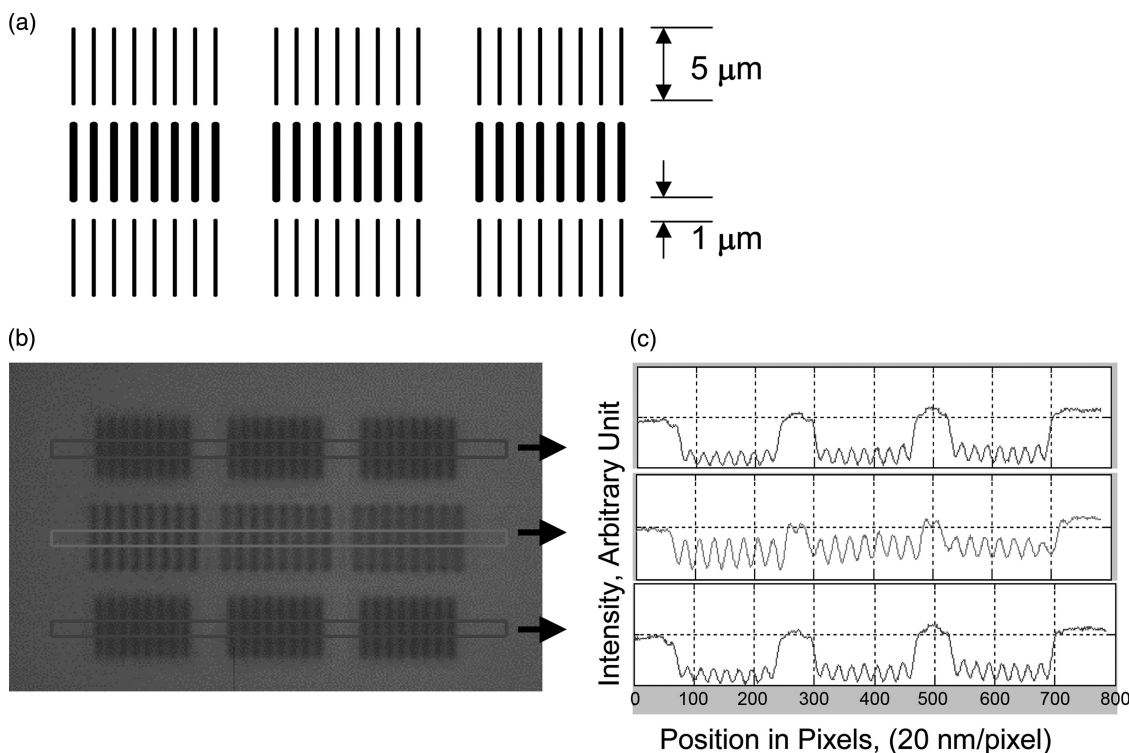
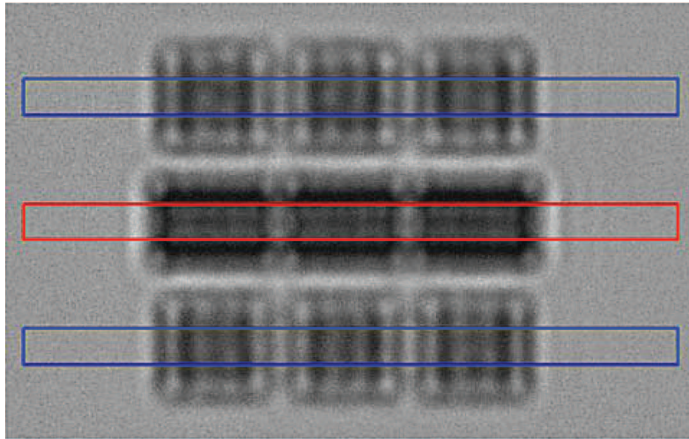


Fig. 5. (a) Schematic of the target designs. This is one example of several variations of this design. (b) Image and a set of profiles for a target, which reflects higher-order optical content. On the wafer there are five target pitches and three offset values, 0,  $\pm 10$  nm.

## Overlay measurements on targets with only zero-order central response



**Nominal feature sizes are 50 nm CD  
With 270 nm pitch.**

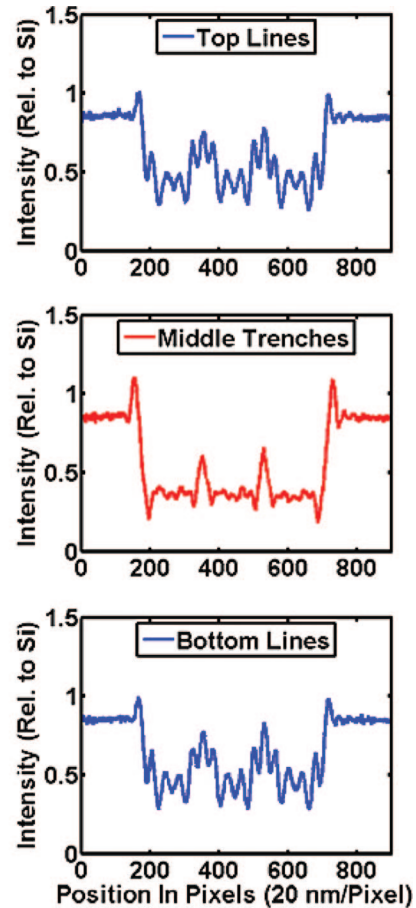


Fig. 6. (Color online) An image with zero-order scattering characteristics for all targets is shown on the left. The data windows from the image are plotted on the right side. This is a standard target with no designed-in CD variation. The intensity oscillations, observed as the four bars in the top row and bottom row of targets, is an edge-based interference effect. This is the result of the optical proximity of the array edges, which interfere with one another. Larger target arrays with the same linewidth dimensions and spacing demonstrate the expected constant intensity in the central array region.

the highest illumination angles in images with significantly increased high-frequency image content. Using this approach with dipole illumination for single-axis overlay metrology or quadrupole illumination for two-dimensional measurements can enable symmetric image profiles with higher-order content.

### B. Arrayed Target Scanning Measurements

Acquiring data as described in Section 3 by incrementing the illumination angle and acquiring images as the aperture is stepped across the back focal plane allows the entire set of line arrays to be analyzed simultaneously. Using the scanned aperture approach in Section 3 with these targets enables simultaneous analysis of the nine arrays of lines. To evaluate this approach and test sensitivity, a special high-resolution target array was designed, which is called the arrayed linearity target. This target has built-in CD variations across the field of view. Each row of line sets in the target has a different design CD. Figure 8 shows the normal incidence  $0^\circ$  illumination image data with profiles for three different design CDs as described above. In these data, the design increments are 5 nm and the average nominal

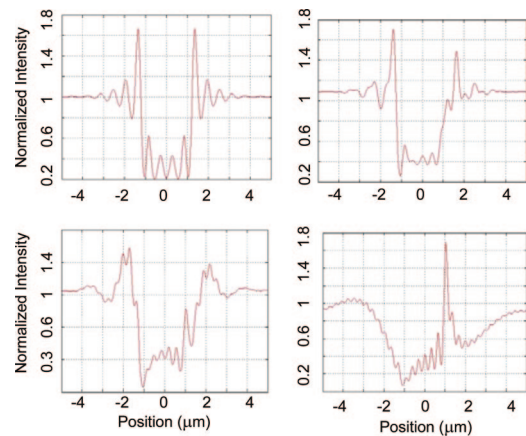


Fig. 7. (Color online) Different panels showing the image as a function of illumination angle, from normal incidence to  $60^\circ$  in  $20^\circ$  increments. The vertical axes are normalized intensity and the horizontal axes are lateral position in micrometers. At the high illumination angles, the higher-order diffraction orders are rocked into the collection optics. A dipole or alternative symmetric illumination can yield symmetric profiles or overlay measurements with higher-order optical content, which would otherwise only show zero-order response.

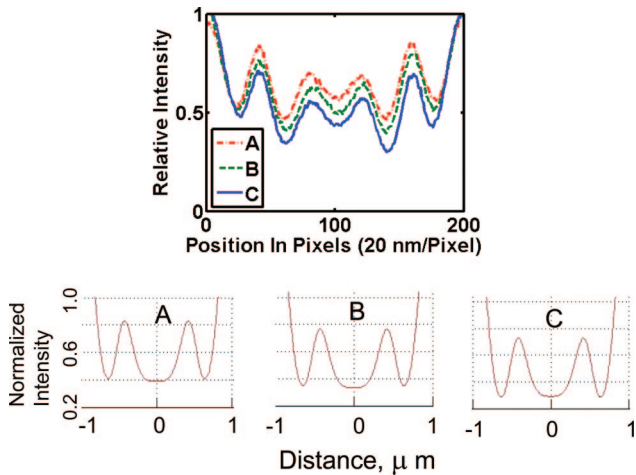


Fig. 8. (Color online) Normalized intensity versus position from three windows in a linearity target having only zero-order response from the eight line target arrays. Simulation results are shown on the bottom and experimental data on top. The mean intensity from the central part of each profile can be analyzed for sensitivity to changes in CD. The experimental results and simulations show the same nominal change in average intensity.

CDs measured by AFM and SEM are 55, 60, and 65 nm. From this image an average intensity is determined for the central region for each profile. Experimental data are shown on the top, and the bottom panels show theoretical results. This is not meant to be a rigorous comprehensive modeling treatment for this target, but rather a demonstration of principle. From each image acquired at a given illumination angle, the resulting profile is analyzed to determine

an average integrated intensity (AII) value for the central target region. Both the experimental results and simulation data show approximately 10 percent changes in the AII for each increment in linewidth. These curves are normalized to background although no silicon reflectivity corrections have been applied.

A complete set of angle-resolved data for the center is shown in Fig. 9. The upper data set is for a non-incremented  $3 \times 3$  overlay target and the lower set is for an incremented linearity target. The upper data show no substantial variation in optical response across the target, whereas the lower set shows a clear monotonic response to the changes in linewidth across the target. The data from Fig. 8 are representative of the  $0^\circ$  illumination angle from the center of the *p*-polarized plot. The data clearly indicate the importance of polarization with respect to sensitivity to change in linewidth.

### 5. Discussion

Although gaps remain in the agreement between the theory and experiment, the sensitivity and resolution are well predicted by the simulations and observed experimentally. The importance of the angle scanning technique is that we can now measure differences in targets with resolution limits well beyond the conventional Rayleigh limit. In fact, the fundamental resolution limits are unclear at this time. The specular component contains quantitative information specific to the feature dimensions, and much recent work in scatterometry shows that measurement resolution and sensitivity will ultimately approach the molecular level.

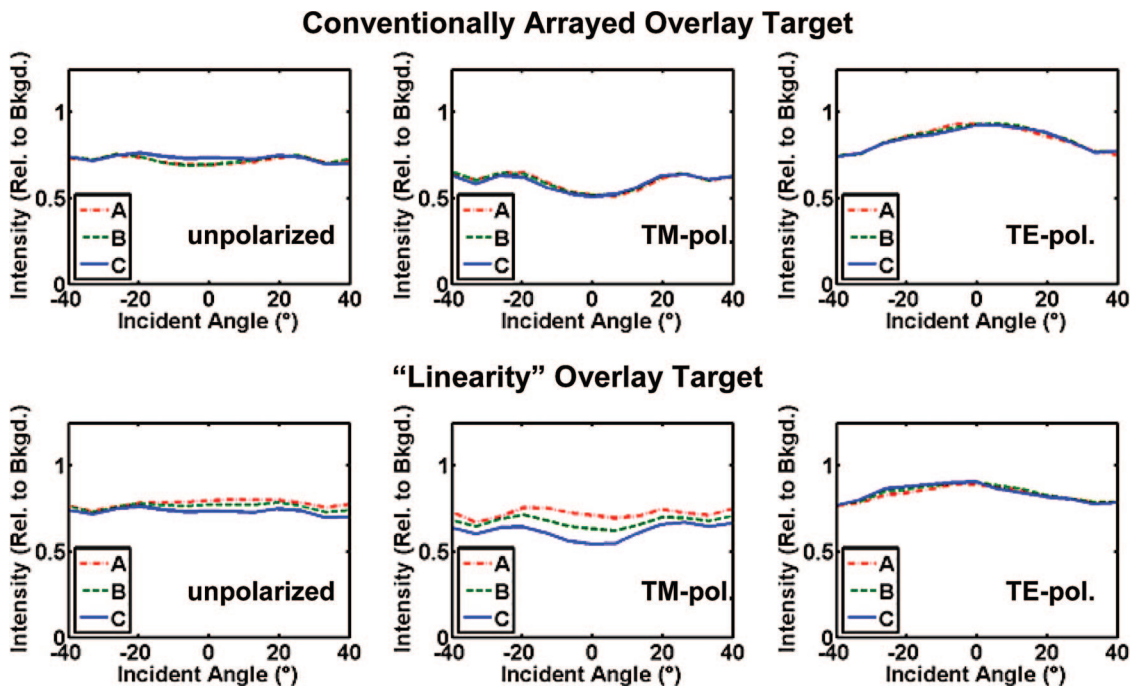


Fig. 9. (Color online) Angle-resolved intensity plots for the center locations in the target patterns. The upper set of panels are for targets with no CD variations designed in and the lower set show 5 nm increments in CD across the target. The *p* polarization shows the best sensitivity. These are complete angle scan data sets.

Significant research has occurred over the years to close the gap in the theoretical understanding of the imaging and electromagnetic scattering processes. Inaccuracies in the model inputs are one significant cause of experiment to model discrepancies. An important component of this work is the ability to measure the illumination as a function of angle, which allows a quantitative evaluation of the polarization dependence of the light as it traverses the optical train. Likewise, the ability to structure and measure the illumination has provided significant insight into the degree that Köhler illumination is achieved in the optical microscope. Additionally, the simplified illumination fields become an important tool to evaluate the effects of aberration and misalignment on the illumination fields and the resulting optical images or optical signatures in the case of a scanned aperture measurement.

## 6. Summary and Conclusions

In this paper we have presented a new technique that combines traditional optical imaging techniques and scanned illumination fields. This was accomplished by scanning an aperture in a conjugate illumination back focal plane. We applied these methods to full-field arrays as well as a new generation of high-resolution targets that can serve as combined overlay and line-width metrology targets. The new target designs were fabricated by SEMATECH and included arrayed features at device sizes as small as 50 nm with target densities from isolated to 1–2 line-space ratios. Our imaging approach was demonstrated on features significantly smaller than predicted by conventional Rayleigh resolution limits. A set of specialized linearity targets having designed-in CD variations were analyzed using both experimental and theoretical analysis.

In analyzing the data from these targets we gain direct insight into the fundamental optical limits from both experimental and theoretical perspectives. This measurement technique, based on an optical signature rather than an edge-based approach, has allowed us to substantially extend the measurement limits with respect to feature dimensions, feature-to-feature distance, and the ability to resolve the difference between two similar target geometries. The data show that by engineering the illumination fields and target designs, accurate measurements of sub-20-nm-sized features may well be attainable.

We acknowledge useful discussions with Tom Germer and Nien Fan Zhang of NIST. We are grateful for metrology, wafer fabrication, and AFM and SEM support from Pete Lipscomb and Mike Bishop from SEMATECH and also acknowledge Mark Davidson for useful discussions and modeling support. We thank the Office of Microelectronics Programs and the Scatterfield Competence Project, both from NIST, for the financial support of this effort.

## References

1. R. Attota, R. M. Silver, M. Bishop, E. Marx, J. Jun, M. Stocker, M. P. Davidson, and R. Larrabee, "Evaluation of new in-chip and arrayed line overlay target designs," *Proc. SPIE* **5375**, 395–402 (2004).
2. J. Seligson, M. Adel, P. Izikson, V. Levinski, and D. Yaffe, "Target noise in overlay metrology," *Proc. SPIE* **5375**, 403–412 (2004).
3. E. Solecky and J. Morillo, "Simultaneous critical dimension and overlay measurements on a SEM through target design for inline manufacturing lithography control," *Proc. SPIE* **5375**, 41–50 (2004).
4. R. M. Silver, R. Attota, M. Stocker, M. Bishop, L. Howard, T. Germer, E. Marx, M. Davidson, and R. Larrabee, "High-resolution optical metrology," *Proc. SPIE* **5752**, 67–79 (2005).
5. R. M. Silver, R. Attota, M. Stocker, M. Bishop, J. Jun, E. Marx, M. Davidson, and R. Larrabee, "High-resolution optical overlay metrology," *Proc. SPIE* **5375**, 78–95 (2004).
6. R. Attota, R. M. Silver, T. Germer, M. Bishop, R. Larrabee, M. Stocker, and L. Howard, "Application of through-focus focus-metric analysis in high resolution optical microscopy," *Proc. SPIE* **5752**, 1441–1449 (2005).
7. R. M. Silver, R. Attota, M. Stocker, J. Jun, E. Marx, R. Larrabee, B. Russo, and M. Davidson, "Comparison of measured optical image profiles of silicon lines with two different theoretical models," *Proc. SPIE* **4689**, 409–429 (2002).
8. M. Bishop, R. Silver, and B. Bunday, "The OMAG 3 reticle set," Tech Transfer #03074417A-ENG (International SEMATECH, 2004).
9. C. M. Herzinger, B. Johs, W. A. McGahan, J. A. Woolam, and W. Paulson, "Ellipsometric determination of optical constants for silicon and thermally grown silicon dioxide via a multi-sample, multi-wavelength, multi-angle investigation," *J. Appl. Phys.* **83**, 3323–3336 (1998).
10. R. M. Silver, B. Barnes, R. Attota, J. Jun, J. Filliben, J. Soto, M. Stocker, P. Lipscomb, E. Marx, H. Patrick, R. Dixon, and R. Larrabee, "The limits of image-based optical metrology," *Proc. SPIE* **6152**, 6152OZ (2006).
11. E. Marx and J. Potzick, "Simulation of optical microscope images of photomask feature size measurements," in *IEEE Antennas and Propagation Society International Symposium (IEEE, 2005)*, Vol. 3B, pp. 243–246.
12. M. Davidson, B. H. Kleemann, and J. Bischoff, "A comparison between rigorous light scattering methods," *Proc. SPIE* **305**, 606–619 (1997).